Electronic Supplementary Material (ESI) for Physical Chemistry Chemical Physics.

Electronic Supplementary Information for: Helical versus linear helical Jahn-Teller distortions in allene and spiropentadiene radical cations

Marc H. Garner, Ruben Laplaza, and Clemence Corminboeuf*

Laboratory for Computational Molecular Design, Institute of Chemical Sciences and Engineering, Ecole Polytechnique federale de Lausanne (EPFL), 1015 Lausanne, Switzerland.

E-mail: clemence.corminboeuf@epfl.ch

Normal Modes of Stationary Points

In the introduction of the manuscript we discuss the D_2 and C_{2v} stationary points of the allene and spiropentadiene radical cations. In Table S1 and S2 we list the first 5 normal modes of the frequency analysis computed with the ωB97X-D functional and the def2-TZVP basis in Gaussian16.[1–3] In both systems the D_2 structures are the global minima with no imaginary frequencies. In allene, the C_{2v} stationary point is a 1st order saddle point with where the torsion mode is an imaginary frequency, see also the in-depth work of Schulenberg and Merkt.[4,5] In spiropentadiene, the C_{2v} stationary point is a 2nd order saddle point with two imaginary vibrational modes. The C_{2v} stationary point failed to optimize to fully meet the *tight* optimization criteria; the *maximum displacement* criteria only reaches 0.000184 with the *tight* threshold being 0.000060, but is within the standard threshold of 0.001800. The torsion mode is at -218 cm^{-1}, and a bending mode around the central spiro carbon is at -169 cm^{-1}.

Table S1: First 5 normal modes of D_2 and C_{2v} structures of allene cation.

	D_2	C_{2v}
v_1	323 cm^{-1}	-1167 cm^{-1}
v_2	342 cm^{-1}	327 cm^{-1}
v_3	784 cm^{-1}	333 cm^{-1}
v_4	805 cm^{-1}	763 cm^{-1}
v_5	922 cm^{-1}	891 cm^{-1}

Table S2: First 5 normal modes of D_2 and C_{2v} structures of spiropentadiene cation.

	D_2	C_{2v}
v_1	305 cm^{-1}	-218 cm^{-1}
v_2	360 cm^{-1}	-169 cm^{-1}
v_3	380 cm^{-1}	364 cm^{-1}
v_4	570 cm^{-1}	381 cm^{-1}
v_5	589 cm^{-1}	654 cm^{-1}

CASPT2 Computations

Allene and spiropentadiene radical cations are optimized with D_2 and C_{2v} symmetry constraint using CASPT2 with cc-pVDZ as implemented in OpenMolcas.[6,7] State-averaged CASSCF is used to optimize the wavefunctions that are used in the CASPT2 computation.

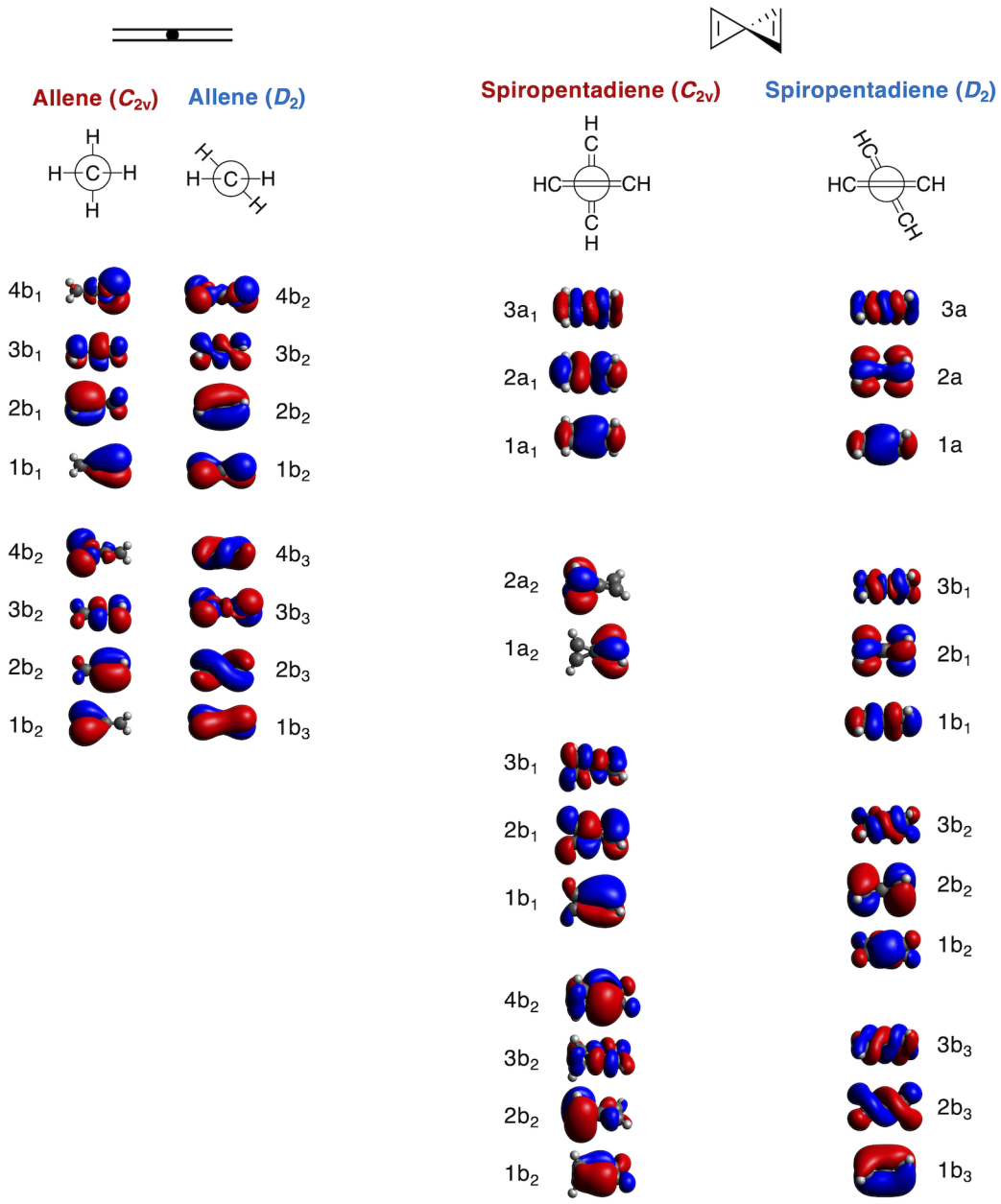

Figure S1: Active spaces (CASSCF MOs) for C_{2v} and D_2 allene and spiropentadiene radical cations.

Shown in the left half of Figure S1, (7,8) active spaces were chosen for the two allene cation structures to cover their π-spaces, as well as the hydrogen s-orbitals that hyperconjugate into the π-system. The C_{2v} ground-state is 94% SCF doublet state with singly-occupied $2b_2$. The D_2 ground-state is 94% SCF doublet state with singly-occupied $2b_3$.

Shown in the right half of Figure S1, (11,12) active spaces were chosen for the two spiropentadiene cation structures to cover their π-spaces. The active space further covers σ-orbitals on the spiro-carbon and double-bonds, which can mix into the π-system when the symmetry is reduced. The C_{2v} ground-state is 88% SCF doublet state with singly-occupied $2b_1$. The D_2 ground-state is 88% SCF doublet state with singly-occupied $2b_3$.

Tolane, Diboracumulenes and Borynes

We find few issues for the simple mnemonic which relates the number of π electrons to the structure of linear molecules also accounts for. A challenge arises in systems where there is no intuitive way to segment the molecule into a separate linear component. In diphenylacetylene (tolane) the torsion barrier is 0.6 kcal/mol and the energy difference between the co-planar and perpendicular conformation is thus negligible.[8,9] How does one segment tolane? We can put 6 π-electrons into the linear part, leaving 5 in each phenyl ring; this correctly predicts the co-planar structure. Or we envision 6 π-electrons localized in each phenyl ring, which leaves 4 π-electrons in the linear segment that gives a perpendicular orientation of the rings. The co-planar arrangement turns out to be the slightly more stable one.[8,9]

The disputed cases of chemical bonding in diboracumulenes and borynes, which were reported by Braunschweig and co-workers, are also well-accounted for.[10–13] Structurally they are similar to diaminoacetylene in the sense that the number of π-electrons differs from the equivalent all-carbon systems due to heteroatoms.[14] In the electron-deficient bora-systems the heteroatoms are in the center of the linear chain. Both diboracumulenic and borynic molecules have perpendicular end-groups. The diboracumulenic structure is understood in terms of the usual π-bonding picture. The borynic structure can be understood as the terminal N-heterocyclic carbene rings having 6 π-electrons. This allows the carbene lone-pair to form a dative bond into the boryne moeity.[15–19]

The difference between diboracumulene and boryne is also straightforward to derive from the frontier MOs,[10,11,20] which are shown in rectilinear and helical representations in Figure S2a. In dibora[3]cumulene the HOMO and HOMO-1 have bonding character across each of the C-B double-bonds. In the boryne these switch place energetically with the LUMO and LUMO$+1$, so that the HOMO and HOMO-1 instead have bonding character across the B-B bond. The helical and rectilinear representations of the MOs are no different in this regard, but it may be visually clearer from the rectilinear MOs when a 3D-rotable picture is not available.

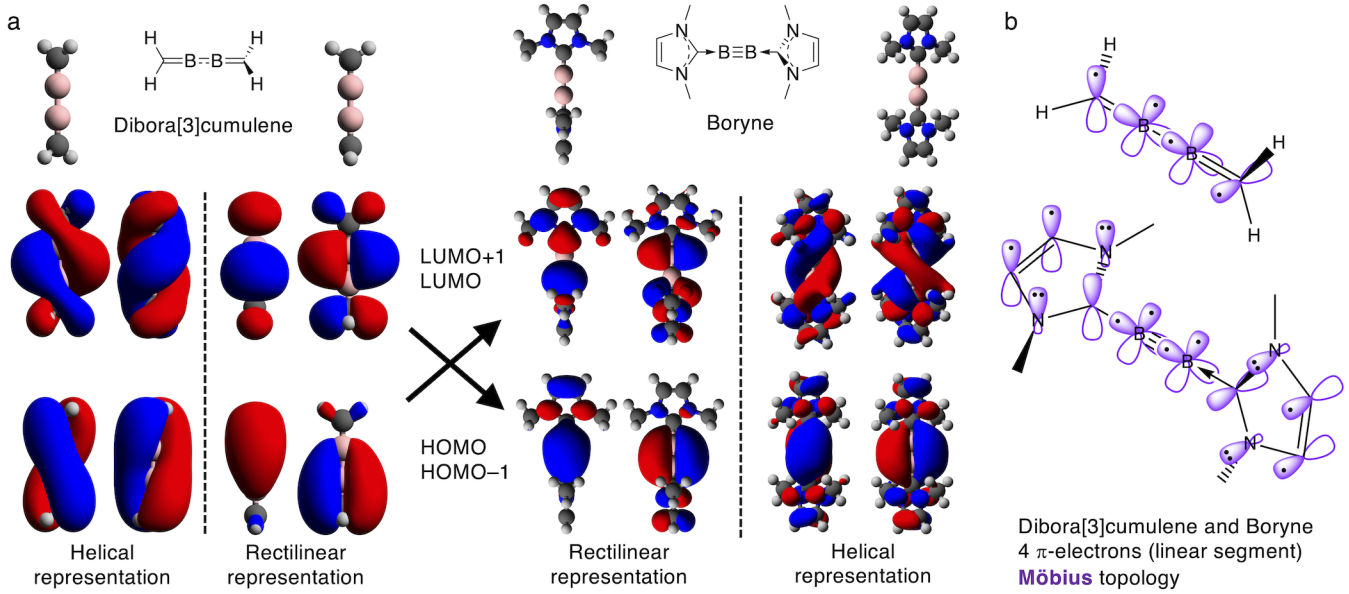

Figure S2: a) Optimized structures and HOMO-1 to LUMO+1 in both their two symmetry-adapted versions of D_{2d} bora[3]cumulene and boryne. b) Schematic overview of number of π-electrons in the linear segments of dibora[3]cumulene and boryne.

The change in bonding from the bora[3]cumulene to the boryne in Figure S2a has notable effect on the molecular structure. The C-B bond lengths change from 1.49 Å to 1.39 Å, and the B-B bond length from 1.45 Å to 1.59 Å. Despite the quite different bonding motifs and change of occupation in the frontier MOs, the end-groups remain perpendicular in both systems. When we draw up the coarctate orbital bases in Figure S2b, we may realize that in both cases there are 4 π-electrons in the linear segments of the molecules. Because the π-electron count does not change, the molecules have similar geometries. Both adopt a perpendicular structure to achieve Möbius topology.

Frontier MOs During Torsion

The frontier MOs of D_2 and C_{2v} Allene and spiropentadiene radical cations are shown at different dihedral angles in Figure S3. The corresponding eigenvalue and energy profiles are shown in Figure 9 in the manuscript. While the D_2 structures have helical MOs at both 60° and 90°, the C_{2v} structure have rectilinear π-MOs at 90° and helical MOs at 60°.

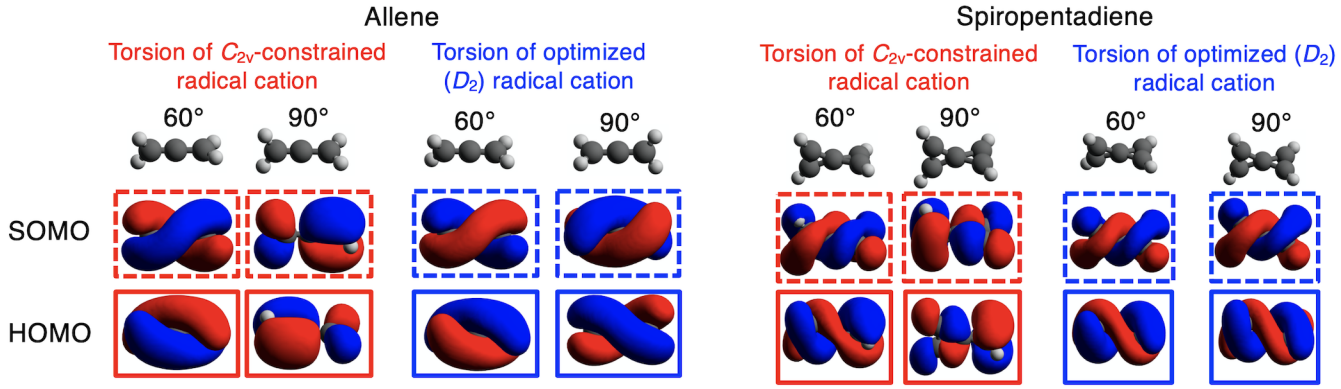

Figure S3: Frontier MOs of allene and spiropentadiene radical cations computed at different torsion angles starting from the optimized D_2 and constrained C_{2v} structures. The SOMO and doubly-occupied HOMO are shown at 60° and 90° torsion angle.

References

(1) Chai, J.-D.; Head-Gordon, M. Long-range corrected hybrid density functionals with damped atomâatom dispersion corrections. *Phys. Chem. Chem. Phys.* **2008**, *10*, 6615–6620.

(2) Weigend, F.; Ahlrichs, R. Balanced basis sets of split valence, triple zeta valence and quadruple zeta valence quality for H to Rn: Design and assessment of accuracy. *Phys. Chem. Chem. Phys.* **2005**, *7*, 3297–3305.

(3) Frisch, M. J.; Trucks, G. W.; Schlegel, H. B.; Scuseria, G. E.; Robb, M. A.; Cheeseman, J. R.; Scalmani, G.; Barone, V.; Petersson, G. A.; Nakatsuji, H. et al. Gaussian 16 Revision A.03. 2016; Gaussian Inc. Wallingford CT.

(4) Schulenburg, A. M.; Merkt, F. Rotationally resolved photoelectron spectroscopic study of the Jahn–Teller effect in allene. *J. Chem. Phys.* **2009**, *130*, 034308.

(5) Schulenburg, A.; Merkt, F. Internal rotation in Jahn–Teller coupled systems: The ethene and allene cations. *Chem. Phys.* **2010**, *377*, 66–77.

(6) Fdez. Galván, I.; Vacher, M.; Alavi, A.; Angeli, C.; Aquilante, F.; Autschbach, J.; Bao, J. J.; Bokarev, S. I.; Bogdanov, N. A.; Carlson, R. K. et al. OpenMolcas: From Source Code to Insight. *J. Chem. Theory Comput.* **2019**, *15*, 5925–5964, PMID: 31509407.

(7) Aquilante, F.; Autschbach, J.; Baiardi, A.; Battaglia, S.; Borin, V. A.; Chibotaru, L. F.; Conti, I.; De Vico, L.; Delcey, M.; Fdez. Galván, I. et al. Modern quantum chemistry with [Open]Molcas. *J. Chem. Phys.* **2020**, *152*, 214117.

(8) Okuyama, K.; Hasegawa, T.; Ito, M.; Mikami, N. Electronic spectra of tolan in a supersonic free jet: large-amplitude torsional motion. *J. Phys. Chem.* **1984**, *88*, 1711–1716.

(9) Thulstrup, P. W.; Hoffmann, S. V.; Hansen, B. K. V.; Spanget-Larsen, J. Unique interplay between electronic states and dihedral angle for the molecular rotor diphenyldiacetylene. *Phys. Chem. Chem. Phys.* **2011**, *13*, 16168–16174.

(10) Braunschweig, H.; Dewhurst, R. D.; Hammond, K.; Mies, J.; Radacki, K.; Vargas, A. Ambient-Temperature Isolation of a Compound with a Boron-Boron Triple Bond. *Science* **2012**, *336*, 1420–1422.

(11) Böhnke, J.; Braunschweig, H.; Ewing, W. C.; Hörl, C.; Kramer, T.; Krummenacher, I.; Mies, J.; Vargas, A. Diborabutatriene: An Electron-Deficient Cumulene. *Angew. Chem. Int. Ed.* **2014**, *53*, 9082–9085.

(12) Böhnke, J.; Braunschweig, H.; Constantinidis, P.; Dellermann, T.; Ewing, W. C.; Fischer, I.; Hammond, K.; Hupp, F.; Mies, J.; Schmitt, H.-C. et al. Experimental Assessment of the Strengths of B-B Triple Bonds. *J. Am. Chem. Soc.* **2015**, *137*, 1766–1769.

(13) Arrowsmith, M.; Braunschweig, H.; Stennett, T. E. Formation and Reactivity of Electron-Precise B-B Single and Multiple Bonds. *Angew. Chem. Int. Ed.* **2017**, *56*, 96–115.

(14) Balakrishnan, A.; Vijayakumar, S. Highly delocalised molecular orbitals in boron-, carbon- and nitrogen-based linear chains: a DFT study. *Mol. Phys.* **2022**, e2020923.

(15) Köppe, R.; Schnöckel, H. The boron-boron triple bond? A thermodynamic and force field based interpretation of the N-heterocyclic carbene (NHC) stabilization procedure. *Chem, Sci.* **2015**, *6*, 1199–1205.

(16) Perras, F. A.; Ewing, W. C.; Dellermann, T.; Böhnke, J.; Ullrich, S.; Schäfer, T.; Braunschweig, H.; Bryce, D. L. Spying on the boron-boron triple bond using spin-spin coupling measured from ^{11} B solid-state NMR spectroscopy. *Chem. Sci.* **2015**, *6*, 3378–3382.

(17) Holzmann, N.; Hermann, M.; Frenking, G. The boron-boron triple bond in NHC-BB-NHC. *Chem. Sci.* **2015**, *6*, 4089–4094.

(18) Mierzwa, G.; Gordon, A. J.; Berski, S. The nature of the triple B B, double, B B, single, B-B, and one-electron, BB boron-boron bonds from the topological analysis of electron localisation function (ELF) perspective. *J. Mol. Struc.* **2020**, *1221*, 128530.

(19) Gorantla, S. M. N. V. T.; Pan, S.; Mondal, K. C.; Frenking, G. Revisiting the Bonding Scenario of Two Donor Ligand Stabilized C2 Species. *J. Phys. Chem. A* **2021**, *125*, 291–301.

(20) Xu, C.; Ma, Y.; Cheng, L. Revisiting the π-Back-Donation in the NHC-B-B-NHC Molecule. *J. Phys. Chem. A* **2021**, *125*, 1681–1687.